Polymer Testing 65 (2018) 468–479

Contents lists available at ScienceDirect

Polymer Testing

journal homepage: www.elsevier.com/locate/polytest

Poly(butylene succinate)-cellulose triacetate blends: permeation, pervaporation, sorption and physical structure

Petr Číhal[a], Ondřej Vopička[a,*], Marek Lanč[a], Miroslav Kludský[a], Jiří Velas[a], Zdeněk Hrdlička[b], Alena Michalcová[c], Marcela Dendisová[a], Karel Friess[a]

[a] Department of Physical Chemistry, University of Chemistry and Technology, Prague, Technická 5, 166 28 Prague 6, Czech Republic
[b] Department of Polymers, University of Chemistry and Technology, Prague, Technická 5, 166 28 Prague 6, Czech Republic
[c] Department of Metals and Corrosion Engineering, University of Chemistry and Technology, Prague, Technická 5, 166 28 Prague 6, Czech Republic

ARTICLE INFO

Keywords:
PBS CTA blends
Barrier properties
Glass transition
Physical properties
Pervaporation and permeation

ABSTRACT

We report on the characterization of blends of polybutylene succinate (PBS) with cellulose triacetate (CTA) with focus on their mass transport properties and physical structure. Blends containing 0–30 wt% of PBS were tested using gas permeation, vapour permeation, pervaporation and vapour sorption. Permeability for gases (CO_2, H_2, etc.) de creased with increasing PBS content in a fixed ratio. In contrast to that, permeability for vapours (methanol, dimethyl carbonate) decreased compound-specifically, thus rendering the blends more selective towards methanol than pure CTA. Interestingly, higher separation factors were observed for the permeation of vapours than for the pervaporation of liquids. The influence of the PBS content on the physical structure and thermal properties of the blends were studied using XRD, SEM, FTIR-ATR, DSC, TGA and DMA techniques. Overall, the blends of PBS and CTA were homogenous, thermally stable and had enhanced barrier properties compared to pure CTA.

1. Introduction

Cellulose triacetate (CTA) has been frequently used as a basic material for numerous applications in packaging, coating and production of separation membranes [1–9]. Recently, Uesaka et al. [10] reported that polybutylene succinate (PBS) forms homogenous blends with CTA. The authors observed that crystallisation of PBS is completely hindered in blends containing less than 40 wt% of PBS and that these blends are homogenous and stable up to 170 °C. Similar properties were later observed also for blends of cellulose acetate butyrate with PBS and its analogues [11,12]. Since CTA is a basic material for the above mentioned applications, its blending with PBS represents an attractive alternative route of modifying its barrier and separation properties. Despite that, neither transport nor barrier properties of PBS-CTA have been reported in the available literature. Moreover, as PBS and CTA easily degrade in nature [10,13], their further exploitation could contribute the overall environmental sustainability of the economy.

Acetates of cellulose are classical materials for the production of packaging films and membranes for separations of gases, vapours and liquids [2,3,5,9]. Therefore, we report on the permeation of common gases, vapours and liquids through thin films made from PBS-CTA blends containing 0–30 wt% of PBS. Namely, the studied gases were carbon dioxide, hydrogen, helium, methane, oxygen, nitrogen and argon. The studied vapours and liquids were methanol and dimethyl carbonate (DMC). Membrane separation of the latter compounds is of interest since DMC is an environment-friendly “green” solvent and chemical intermediate that is produced from methanol with which it forms azeotrope [14,15]. To separately study diffusion and dissolution of methanol and DMC in the blends, vapour sorption tests were performed with these compounds. Additionally, sorption of methyl acetate (MeOAc), which is a structural analogue of DMC, was characterized to disclose the influence of a “small” change in the chemical structure of the probing compound.

Since potentially meaningful materials for membrane separations should withstand temperatures above 100 °C [16], the blends were studied by means of differential scanning calorimetry (DSC), thermogravimetry (TGA) and dynamic mechanical analysis (DMA) to survey their thermal and mechanical properties. Besides that, Uesaka et al. [10] observed pronounced crystallisation of PBS in blends containing at least 50 wt% of PBS (main X-ray diffraction band at $2\theta \approx 20^{\circ}$), while crystallisation is hindered below this concentration. We thus report in detail on the physical structure of blends containing 0, 10, 20, 30 wt% of PBS using XRD, scanning electron microscopy (SEM) and Fourier transform infrared-attenuated total reflectance (FTIR-ATR) techniques

* Corresponding author.
E-mail address: ondrej.vopicka@vscht.cz (O. Vopička).

https://doi.org/10.1016/j.polymertesting.2017.12.026
Received 4 August 2017; Received in revised form 11 December 2017; Accepted 22 December 2017
Available online 27 December 2017
0142-9418/

and provide comparison to samples of higher PBS contents. Within the explored concentration region, blending is an interesting way of tailoring the material properties for the applications in which pure CTA has so far been used.

2. Theory of mass transport

Intensity of the steady flux of a gas diffusing through a flat dense membrane can be expressed with integrated Fick's first law [17,18] having form

$$J_i = -P_i \frac{p_i^{\text{perm.}} - p_i^{\text{feed}}}{L}, \tag{1}$$

where $p_i^{\text{perm.}}$ and p_i^{feed} are partial pressures of the gas at the permeate (low pressure) and feed (high pressure) side of the membrane, L is membrane thickness and P the respective permeability. Permeability equals, provided that solution-diffusion model is assumed, to the product of diffusivity and solubility constant. In the case of permeation of vapours, partial pressure can be alternatively expressed in terms of vapour activity: $a_i = p_i/p_i^{\text{sat}}$. Permeation of vapours is closely connected to permeation of liquids, usually referred to as pervaporation. Thus, in analogy to Eq. (1), the expression of the flux intensity for pervaporation takes [19] the form

$$J_i = -P_i \frac{p_i^{\text{perm.}} - p_i^{\text{sat.}}\, \gamma_i^{\text{feed,liq}} x_i^{\text{feed,liq.}}}{L}, \tag{2}$$

where $\gamma_i^{\text{feed,liq.}}$ and $x_i^{\text{feed,liq.}}$ are activity coefficient and molar fraction of component i in the liquid feed. In this work, activity coefficients in the mixtures of methanol and DMC were taken from literature [15].

In order to determine diffusivity (D) of a compound in a flat membrane, transient sorption of the compound into the initially clean film can be measured. This process can be described using following model [18]:

$$\frac{m_\tau}{m_\infty} = 1 - \frac{8}{\pi^2} \sum_{i=0}^{\infty} \frac{1}{(2i+1)^2} \exp\left[-\frac{(2i+1)^2 \pi^2 D \tau}{L^2} \right]. \tag{3}$$

Equilibrium sorption isotherms of volatile compounds in polymers are typically upward-curved [20] or *S*-shaped [21] and can often be parameterized with Guggenheim–Anderson–De Boer (GAB) model of multilayer adsorption [22] in form:

$$v = \frac{v_m\, h\, f\, a}{(1 - f\, a)(1 - f\, a + h\, f\, a)}, \tag{4}$$

where v is sorption uptake and v_m, h and f are three adjustable parameters having the meanings of monolayer capacity, binding strength constant and a constant measuring the apparent condensability of the sorptive; *i.e.* the departure of its reference pressure from the saturated vapour pressure.

3. Experimental

3.1. Materials and chemicals

Cellulose triacetate (acetyl content 43–44%; *i.e.* degree of substitution 2.78–2.90 [23], Acros Organics) and poly(butylene succinate) (Bionolle 1001 MD, Showa Denko Europe) were used as received. Pellets of the polymers were dissolved in stirred boiling chloroform (stabilized with amylene, min. 99.83%, Lach–ner). Cold solutions containing ca. 0.5 wt% of polymers were cast in glass Petri dishes and covered; solvent evaporation took ca. 4 days. Afterwards, all films were exposed to methanol vapour for ca. two hours and then dried in air to remove the entrapped solvent. Thicknesses of the resulting dense films varied within 30–53 μm; thicker samples (up to 103 μm) were used in the case of pure PBS. Density of CTA, PBS and of all blends was determined by weighing in water and equalled (1.28 ± 0.01) g·cm^{-3}. Gases were used as obtained from SIAD Czech: hydrogen 5.5, helium 4.8, methane 5.5, argon 6.0, nitrogen 4.0, oxygen 2.5 and carbon dioxide 4.0. Methanol (min. 99.8%, Penta), DMC (99+ %, Acros Organics) and MeOAc (min. 99%, Acros Organics) were used as obtained, their physical properties were taken from the database [24].

3.2. XRD, SEM, FTIR-ATR, DSC, TGA and DMA tests

X-ray diffraction analyses were performed using PANalytical X'Pert PRO diffractometer equipped with a copper anode (Cu Kα). In order to mitigate the influence of the film thickness on the diffraction patterns, films having thicknesses of 42 μm ± 10% were used.

Structure of the samples was studied with Scanning Electron Microscopy (SEM) technique using a TESCAN VEGA 3 LMU. Prior to the measurements, samples containing 0–100 wt% of PBS were broken in liquid nitrogen. Fracture surfaces of the samples were then visualized by back scattered electrons (BSE) detector in the Univac mode (used chamber pressure was 10 Pa).

Infrared spectra of the samples were measured using Fourier transform infrared spectrometer Nexus 670 (Thermo Scientific) with an accessory for attenuated total reflectance (FTIR-ATR). Source of mid-infrared radiation (EverGlo, Thermo Scientific), KBr beamsplitter and DTGS detector were used; 128 scans were recorded for each spectrum with the resolution of 2 cm^{-1}. Four spectra were collected for each sample, two points from each side, and then averaged.

Differential scanning calorimetry (DSC) tests were performed using a DSC 4000 from Perkin–Elmer with the linear heating rate of 10 °C min^{-1} and the flow rate of purge and cooling gas (nitrogen) set to 20 ml min^{-1}. Similar to the DSC tests reported by Uesaka et al. [10], each DSC test consisted of temperature scan from 30 °C to 190 °C followed by a prolonged period (5 h) of maintaining the sample at constant temperature (190 °C). Thicker samples (ca. 150 μm, ca. 5 mg, hermetically sealed in aluminium pans) were used in order to ensure sufficient amount of sample and good contact with the thermocouple. The thermograms of the empty aluminium pans were measured alongside and used for correction of their effect. Thermogravimetric tests (TGA) were conducted using a Pyris 1 TGA (Perkin Elmer) with the linear heating rate of 10 °C min^{-1} and with the use of nitrogen as an inert gas.

Measurements of Dynamic Mechanical Analysis (DMA) were performed with a DMA DX04T (RMI). Sinusoidal axial force having the amplitude of 200 mN (average stress 400 kPa) and frequency of 1 Hz was applied to samples containing 0–50 wt% of PBS, while the amplitude of 100 mN (stress 110 kPa) was applied to the sample of pure PBS. Tests were performed in the ambient air atmosphere; temperature was changed at the rate of 3 °C per minute.

3.3. Permeation of gases

Gas permeation measurements were carried out using a fixed-volume pressure-increase apparatus (Fig. 1) at 25 °C. The apparatus was made from duralumin as an evolution of the earlier reported device of this type [25]. The membrane was supported with a sintered steel plate, sealed with a NBR flat O-ring and had the active area of 7.07 cm^2. Tested gas was fed to the membrane at atmospheric pressure. The permeation of gas into the previously vacuumed fixed-volume (permeate) chamber was followed using a pressure gauge (Leybold Ceravac CTR 100 N).

Permeability was calculated [18] based on Eq. (1) and mass

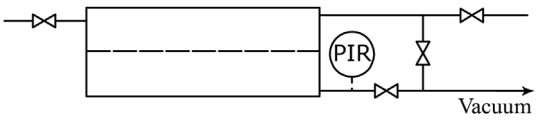

Fig. 1. Scheme of gas permeameter; PIR stands for a pressure sensor with recording.

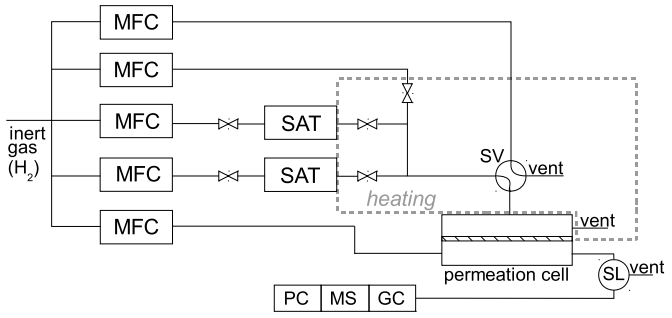

Fig. 2. Scheme of the sweep gas permeameter for vapours [26]. MFC abbreviates mass flow controller, SAT saturator, SV switching valve, SL sampling loop and PC personal computer. Tubes and valves ('cold parts') connecting the saturators and the thermostated cell were heated to ca. 45–55 °C to avoid condensation of vapours.

balance, thus:

$$P = \frac{\mathbf{R}\, T_{STP} L}{A_{mem}\, p_{STP}\, p_{atm}} \cdot \frac{dp}{dt}, \quad (5)$$

where dp/dt is the slope of the pressure increase in the fixed-volume chamber under steady state conditions, A_{mem} is the active area of the membrane, subscript STP indicates standard temperature and pressure: 273.15 K and 101.325 kPa.

3.4. Permeation of vapours

Permeation of binary vapour mixtures of DMC and MeOH was measured using a previously reported continuous mode sweep gas permeameter [26] with the active area of 5.0 cm^2. Vapour mixtures were prepared using two thermostated saturators filled with pure compounds, in which continuous streams of inert gas (hydrogen) were saturated. Activities of individual vapours and composition of the condensable part of the mixture (without hydrogen) were adjusted by adjusting the temperature of the saturators and the respective flow rates of the inert gas (Fig. 2). The final feed mixture was led to the membrane at the atmospheric pressure. Temperature of the measuring cell was 40 °C. Gas chromatograph with mass spectrometer (Clarus 500, Perkin Elmer) was used for permeate analysis and the evaluation of the steady-state flux intensities; hydrogen was used as a sweep gas. Permeabilities of the individual components were consequently calculated using Eq. (1), quantification of DMC and MeOH in permeate were conducted as described elsewhere [26].

Since all tested membranes were selective towards methanol, separation factor was defined as

$$\beta = \frac{x^{perm}_{MeOH}/x^{perm}_{DMC}}{x^{feed}_{MeOH}/x^{feed}_{DMC}}, \quad (6)$$

where x stands for molar fraction of a compound in the respective stream excl. carrier gas.

3.5. Pervaporation

Pervaporation experiments were conducted using a double-jacketed duralumin apparatus, in which hydrogen was used as sweep gas (50 cm^3 (STP) min^{-1}) and active membrane area was 3.14 cm^2. In this setup, the partial pressure of permeate in the sweep gas was lower than 10 kPa. The liquid feed mixture was circulated (ca. 15 $cm^3 s^{-1}$) using a water-jacketed pump containing ca. 150 cm^3 of the mixture, in which pumping was achieved by means of a magnetic stirrer (Fig. 3). The pervaporation cell and feed pump were maintained at (40.0 ± 0.7) °C using a water circulator (modified VEB MLW U). After reaching the steady-state, permeate was collected in a liquid nitrogen cryogenic trap [27] and weighed using an Ohaus DV215CD balance. Permeate and feed were each analysed using a Nicolet iS10 FTIR spectrometer

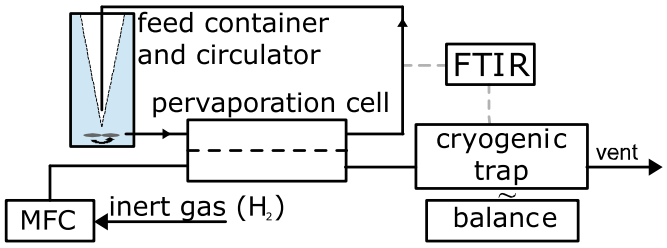

Fig. 3. Scheme of the pervaporation apparatus.

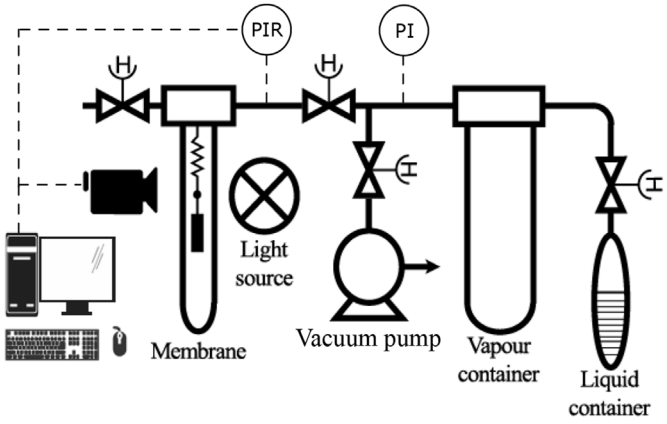

Fig. 4. Scheme of the sorption apparatus; PI and PIR stand for pressure sensors with indication and recording, respectively.

equipped with a gas cell and a MCT/A detector [27]. Permeabilities and separation factors were then calculated based on Eqs. (2) and (6).

3.6. Sorption of vapours

Sorption of vapours was measured using the earlier reported [28] gravimetric sorption apparatus equipped with McBain spiral balances and maintained at 40 °C (Fig. 4). Measured vapour was gradually released into the cell with the sample, which was degassed in vacuum (< 1 Pa) prior to each measurement. The sample was hung on the calibrated quartz spiral, the elongation of which was followed. Tested vapour activities ranged from 0.1 to 0.9.

4. Results and discussion

4.1. Morphology and physicochemical properties

4.1.1. XRD analysis

The XRD pattern of the CTA film (Fig. 5) revealed two overlapping bands peaking at $2\theta \approx 8°$ and 20°, which is in good agreement with the literature [7,9,10,23,29]. The XRD pattern of the PBS film showed two intensive and overlapping bands peaking at $2\theta \approx 20°$ and 23°, and three less intensive bands peaking at $2\theta \approx 29°$, 34° and 39°, which originated from the crystalline nature of PBS [10,28,30–32]. Similar to the work of Uesaka et al. [10], blends containing less than 30 wt% of PBS did not reveal peaks specific for PBS, thus indicating that crystallisation of PBS was hindered. In contrast to that, the blend containing 50 wt% of PBS exhibited peaks typical for PBS crystallites, which coincided with the occurrence of demixing observed by SEM imaging and DMA analysis, see below. Not only the occurrence of the peaks typical for PBS crystallites but also the intensity of the band of CTA at $2\theta \approx 8°$ depended on the PBS content. Indeed, this band ($2\theta \approx 8°$) progressively declined with the increasing PBS loading. In contrast to that, the decrease of the intensity of the band at $2\theta \approx 21°$ was observed [9] upon soaking and consequent plasticization of CTA in glycols. Thus, PBS does not presumably act as a plasticizer but rather causes filling or disarrangement

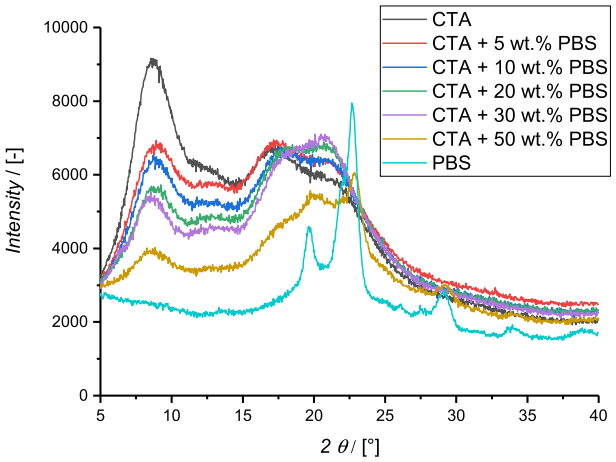

Fig. 5. X-ray diffraction patterns of PBS-CTA and of the respective pure polymers.

of the CTA structures having the apparent spacing of 10.6 Å ($2\theta \approx 8°$).

4.1.2. SEM imaging

Fracture surface micrographs of the films prepared from the pure polymers and blends containing 0–50 wt % of PBS are shown in Fig. 6. Films prepared from the blends containing up to 30 wt% of PBS revealed river patterns typical for amorphous solids, which were similar to those observed for pure CTA (Fig. 6a–d). Unlike that, the films from pure PBS and from the blend containing 50 wt% of PBS revealed pronounced facets typical for intergranular fracture in polycrystalline materials (Fig. 6e and f). Moreover, the break of the blend containing 50 wt% of PBS showed a layered structure, which is presumably a consequence of the limited miscibility of the two polymers having practically equal densities. Overall, blends containing up to 30 wt% of PBS were homogeneous to a comparable extent as pure CTA while the blend containing 50 wt% of PBS was heterogeneous and revealed discernible phase separation.

4.1.3. FTIR-ATR analysis

FTIR-ATR spectra of the films prepared from PBS, CTA and their blends showed that rather minor changes occurred due to blending (Fig. 7). Namely, the increasing content of PBS caused the increase of intensity and broadening of the band of CTA at 1738 cm^{-1} (C═O stretching) due to the presence of the overlapping band of PBS at 1711 cm^{-1} (C═O stretching). Though the hindrance of PBS crystallisation was reported to cause a shift of the latter band towards higher wavenumbers [30], no shift was observed.

4.1.4. DSC and TGA analyses

DSC thermograms were measured so that samples were each heated in nitrogen at a constant rate (10 °C min^{-1}) and then maintained at constant temperature (190 °C) for 5 h. The isothermal thermograms (Fig. 8a) did not fully cohere with those of Uesaka et al. [10] reported for blend containing 30 wt% of PBS as these did not show peaks of delayed demixing. This might be, however, a consequence of using another CTA. Thus, DSC tests confirmed that mixtures containing less than 30 wt% of PBS were thermally stable at temperatures below 190 °C. The sample with 30 wt% of PBS showed a repeatable endothermal peak within the first 2 h of isothermal analysis, which presumably resulted from a more free dispersion of the PBS chains at higher PBS loadings. Consistent with that, (first) temperature scan analysis (Fig. 8b) showed that the endothermal transition was disproportionally more intensive for the blend containing 30 wt% of PBS than for the blends with lower loadings (see values of enthalpy and crystallinity indices of PBS in Table 1). This phenomenon was possibly related to a phase change of the PBS molecules captured inside the CTA matrix despite no PBS crystallites were yet detectable with XRD. Indeed, while pure CTA revealed a non-intensive peak starting at 78.3 °C, this peak became progressively more intensive and shifted towards the melting temperature of PBS (124 °C) with the increasing content of PBS. This peak is thus probably related to the arrangement of the PBS chains within the matrix, which becomes more similar to that in pure PBS at higher PBS loadings.

Thermogravimetric analysis (TGA) was conducted, similar to the

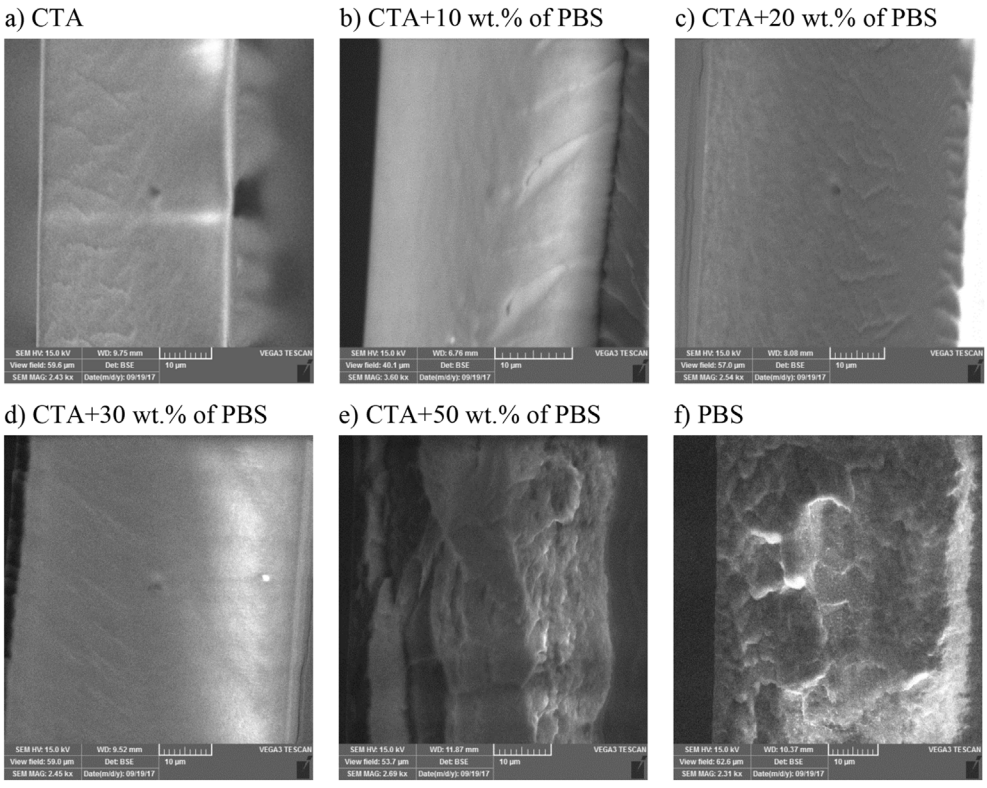

Fig. 6. SEM fracture surface micrographs of films from CTA, PBS and their blends.

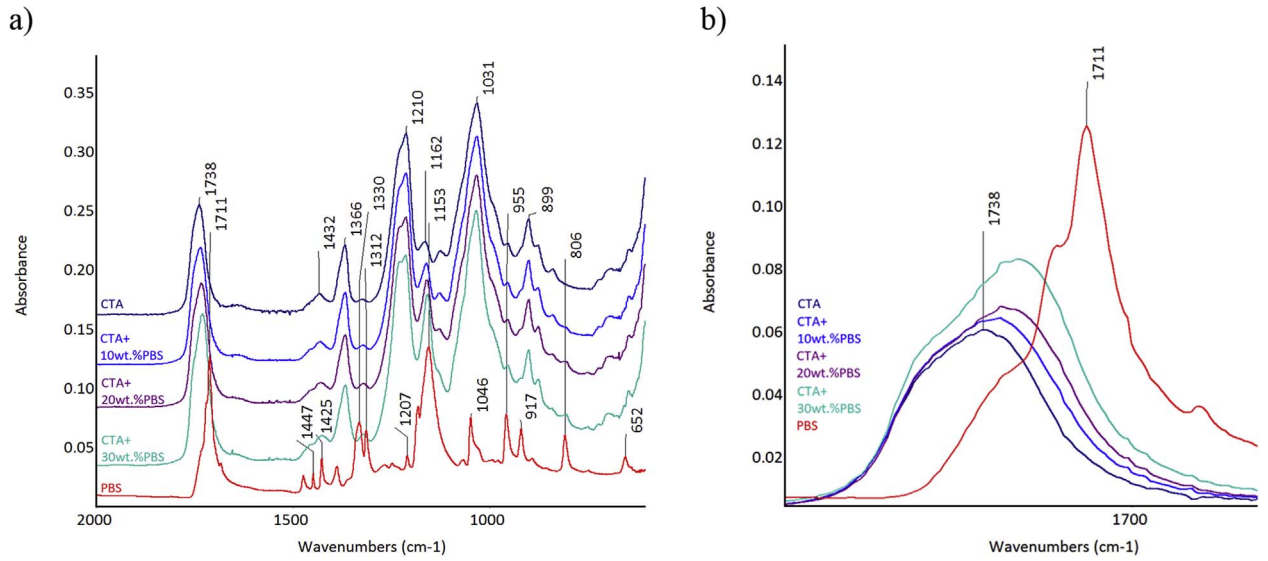

Fig. 7. FTIR-ATR spectra of films from CTA, PBS and their blends (a) and detail of the respective C═O stretching bands (b).

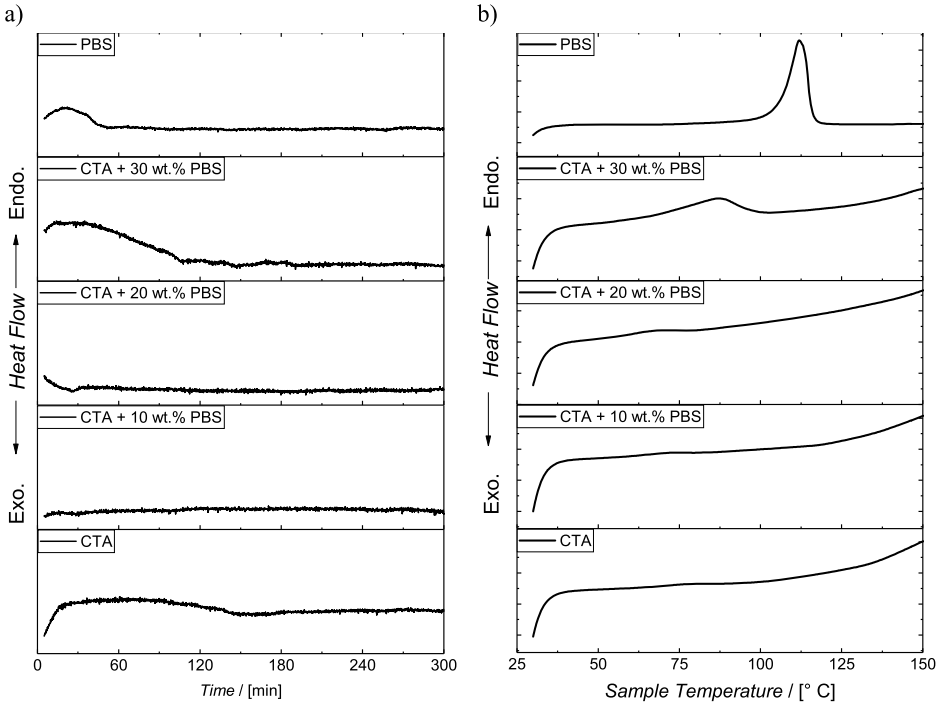

Fig. 8. Isothermal DSC thermograms of CTA, PBS and their blends at 190 °C for 5 h (a) and DSC temperature scans measured at ramp 10 °C min^{-1} (b). Values of Δh from peak analysis are shown in Table 1.

Table 1
Endothermic phase transition properties of PBS-CTA polymeric films evaluated as onsets and integrated DSC peak areas measured at the heating rate of 10 °C min^{-1}, together with the respective crystallinity indices of PBS.

	t_{onset}/[°C]	Δh/[J g^{-1}]	$X_{c,PBS} = \frac{\Delta h_f^{wPBS}}{\Delta h_{f,PBS}^{purePBS} w_{PBS}}$
CTA	78.3	0.58	–
CTA + 10 wt% PBS	72.5	0.63	0.06
CTA + 20 wt% PBS	68.0	0.81	0.04
CTA + 30 wt% PBS	86.8	12.63	0.40
PBS	106.0	105.52	1.00

DSC tests, so that each sample was heated under nitrogen at a constant rate (10 °C min^{-1}) and then maintained at constant temperature (190 °C) for 2 h since no heat flows were detected with DSC at longer times. Rather small changes of weight were observed, as these presumably originated from the loss of entrapped solvent. The highest losses of mass, corrected to the temperature drift, were observed for CTA and for the blends containing 10 and 20 wt% of PBS (Fig. 9), while the smallest changes were observed for blend containing 30 wt% of PBS and for PBS. The increase of mass of CTA observed at temperatures above 100 °C was clearly caused by the temperature drift of the device as nitrogen atmosphere was used. Overall, the observed DSC peaks originated mainly from phase transitions in the condensed phase.

4.1.5. DMA analysis

When subjected to the axial sinusoidal mechanical stress at progressively increasing temperature, all blends revealed maxima of damping, that is glass transitions, at similar temperatures as pure CTA (Fig. 10a), all of which ranged 200–210 °C. Hence, the main compound responsible for the mechanical properties of the blends was CTA.

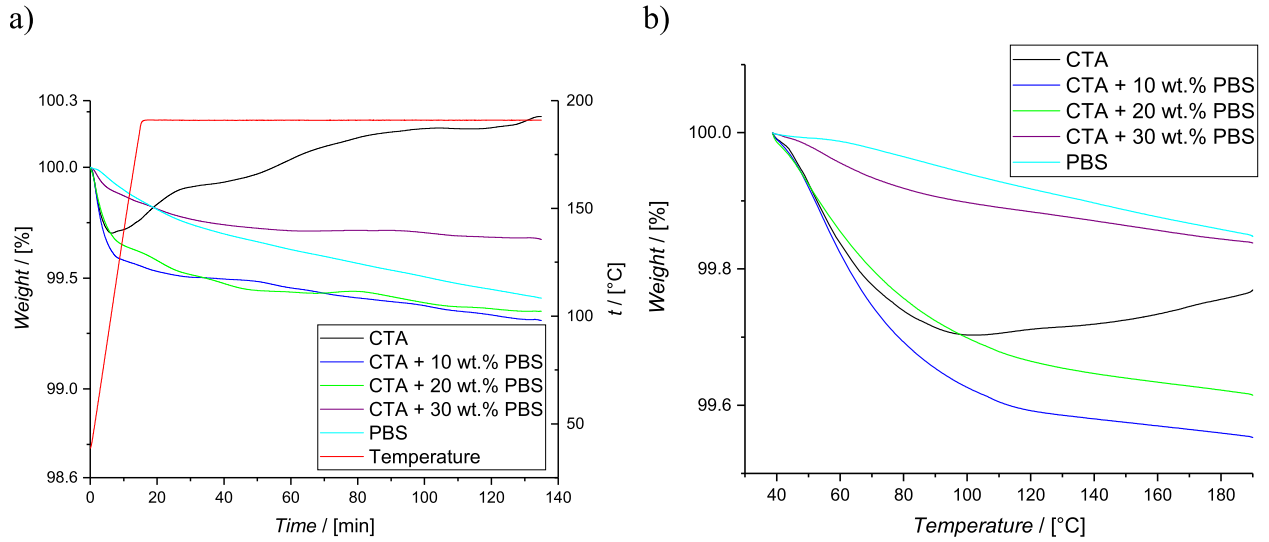

Fig. 9. TGA thermograms of CTA, PBS and their blends (a) and the weight changes within the initial temperature increase (b).

Consistent with the literature [10], the blend containing 50 wt% showed a small but discernible peak of damping at 115 °C, which was presumably so due to the presence of the demixed PBS phase (see section 4.1.2).

Elastic moduli of the blends at low temperatures (35 °C) were of the magnitude typical for glassy polymers (Fig. 10b) and decreased with the increasing content of PBS. Consistent with the literature [10], the elastic moduli decreased with increasing temperature more steeply above ca. 125 °C, that is, above the melting temperature of pure PBS. Hence, entanglements of the two polymers presumably occur in their blends and vanish at temperatures close to or higher than that of PBS melting. The uncertainty of the elastic moduli, estimated based on repeated experiments, was 25%. The melting temperature of pure PBS, observed using the DMA test, equaled 114 °C.

4.2. Permeation of gases

Permeabilities of pure CTA, PBS and their blends for gases are summarized in Table 2. Clearly, PBS-CTA blends exhibited lower gas permeabilities than pure CTA. This is presumably a consequence of the generally very low permeability of PBS, which was immeasurably low for some of the gases. The relationship between gas permeability and the composition of the PBS-CTA blends was highly nonlinear and was correlated with the following empirical model:

Table 2
Permeability of CTA, PBS and PBS-CTA films for gases at 25 °C together with the respective ideal selectivities.

w_{PBS}	P/[Barrer[a]]							Ideal selectivity, P_i/P_j		
	H_2	He	Ar	N_2	O_2	CO_2	CH_4	CO_2/CH_4	O_2/N_2	CO_2/H_2
0	10.2	13.1	0.3	0.3	1.4	5.5	0.1	55	4.7	1.9
0.10	8.0	8.3	0.3	0.2	0.8	3.5	0.1	35	4.0	2.3
0.20	6.6	6.8	0.2	0.2	0.5	3.1	0.2	16	2.5	2.1
0.30	3.8	4.0	0.1	N/A	0.2	1.7	0.1	17	N/A	2.2
1	0.3	0.2	N/A	N/A	N/A	0.3	N/A	N/A	N/A	1.0

N/A stands for immeasurably low permeability and, consequently, for undefined ideal selectivity.
[a] 1 Barrer = 10^{-10} cm^3_{STP} cm cm^{-2} s^{-1} cm Hg^{-1}.

$$P_i^{blend} = w_{CTA} P_i^{CTA} \cdot \exp(-k\, w_{PBS}) + w_{PBS} P_i^{PBS}, \quad (7)$$

where $k = 2.5 \pm 0.5$ for H_2, He, Ar, N_2 and CO_2 and $k = 4.86 \pm 0.02$ for O_2. As an exception, methane permeability of the blends was not correlated to the PBS content, which was presumably so because their permeabilities were comparable to the experimental uncertainty. In Eq. (7), $w_{PBS} = (1 - w_{CTA})$ and $w_{PBS} \varepsilon (0,\ 0.3)$. Similar dependences of gas permeabilities on blend compositions as that expressed here newly with Eq. (7) were reported also for blends of other polymers [33–37]. Thus,

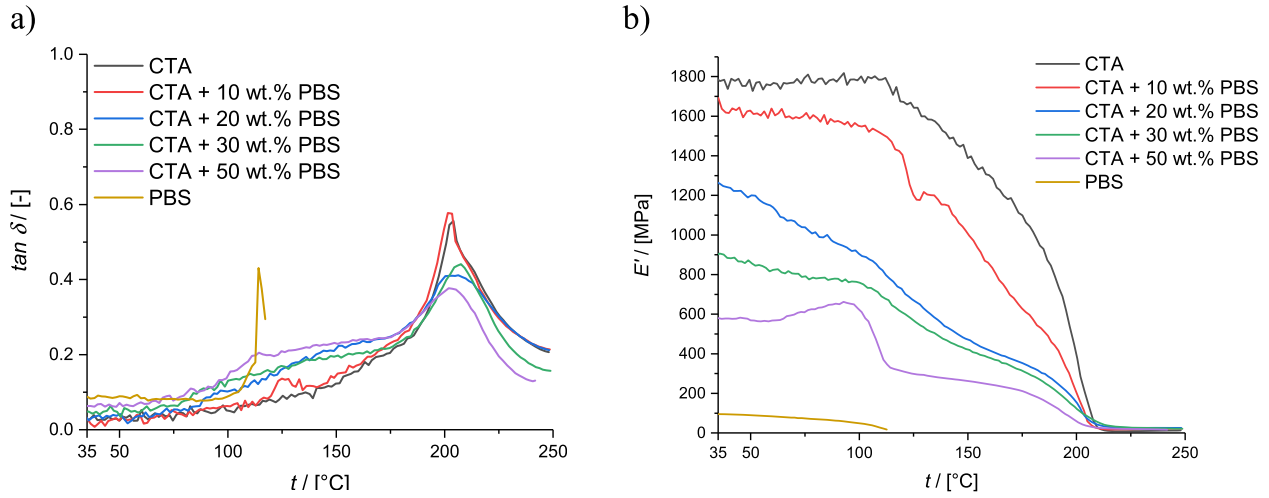

Fig. 10. Temperature dependences of damping (a) and elastic modulus (b) for CTA, PBS and their blends.

Table 3
Permeability (Eq. (1)) and separation factor (Eq. (6)) of CTA and PBS-CTA blends for MeOH-DMC vapour mixtures of given composition, vapour activity and degree of dilution. N/A stands for undetectably low permeability for DMC and, consequently, non-defined separation factors; all at 40 °C.

	x_{MeOH} [−]	a_{MeOH} [−]	a_{DMC} [−]	$p_{feed}^{vap.}/p_{dew\ point}$ [−]	P_{MeOH} [Barrer]	P_{DMC} [Barrer]	β_{MeOH} [−]
CTA	0.62	0.20	0.29	0.30	2556	700	3.65
		0.30	0.43	0.44	2883	967	2.98
		0.40	0.58	0.59	5120	2384	2.15
	0.82	0.20	0.10	0.26	1779	1049	1.70
		0.30	0.16	0.40	1626	920	1.77
		0.40	0.21	0.53	1556	718	2.17
CTA + 5 wt% PBS	0.62	0.20	0.29	0.30	379	41	9.72
		0.30	0.43	0.44	802	197	4.18
		0.40	0.58	0.59	1875	778	2.43
	0.82	0.20	0.10	0.26	331	22	14.93
		0.30	0.16	0.40	377	48	7.78
		0.40	0.21	0.53	424	42	10.07
CTA + 10 wt% PBS	0.62	0.20	0.29	0.30	344	18	19.43
		0.30	0.43	0.44	768	194	4.07
		0.40	0.58	0.59	1964	931	2.16
	0.82	0.20	0.10	0.26	259	N/A (low)	N/A (high)
		0.30	0.16	0.40	281	N/A (low)	N/A (high)
		0.40	0.21	0.53	361	N/A (low)	N/A (high)
CTA + 20 wt% PBS	0.62	0.20	0.29	0.30	298	39	7.94
		0.30	0.43	0.44	727	257	5.90
		0.40	0.58	0.59	1860	1058	1.78
	0.82	0.20	0.10	0.26	171	N/A (low)	N/A (high)
		0.30	0.16	0.40	212	N/A (low)	N/A (high)
		0.40	0.21	0.53	289	N/A (low)	N/A (high)
CTA + 30 wt% PBS	0.62	0.20	0.29	0.30	352	81	4.44
		0.30	0.43	0.44	749	324	2.36
		0.40	0.58	0.59	1783	1137	1.60
	0.82	0.20	0.10	0.26	181	N/A (low)	N/A (high)
		0.30	0.16	0.40	232	N/A (low)	N/A (high)
		0.40	0.21	0.53	346	N/A (low)	N/A (high)

the above model might be applicable to other systems though constant k can, in principle, be specific for the actual penetrants.

As a natural consequence of the existence of the above master curve, only moderate changes of ideal separation selectivity (ratio of single-component permeabilities for two gases) were observed upon changing the PBS loading. Thus, the blends of PBS with CTA did not follow the trend given of the Robeson upper bound [38], according to which a decrease of permeability leads, in the ideal case, to the increase of ideal selectivity.

Overall, the blends of PBS with CTA showed enhanced barrier properties compared to pure CTA, while they were similarly (CO_2/H_2, He/O_2, H_2/O_2) or less selective (CO_2/CH_4, O_2/N_2). However, these blends simultaneously revealed lower sorption of hydrocarbons, see below, thus making them potentially less sensitive to the contaminations of separated gases with vapours or liquids, such as that reported in the literature [9].

4.3. Permeation of vapours and pervaporation

Similar to the permeation of gases, blends of PBS with CTA were less permeable also to vapours and liquids (Tables 3 and 4). In contrast to the permeation of gases, the films from PBS-CTA blends revealed higher separation factors than CTA films in the case of vapour permeation. Besides that, the respective separation factors were not only dependent on the feed mixture composition, but also on the actual vapour activities. Therefore, the separation factors depended on the degree of dilution of the feed mixture. Specifically, the more diluted (depressurized) the vapour mixture was, the smaller were the permeabilities and the higher were the separation factors.

The measurements of the permeation of the vapours were performed at three fixed activities of methanol vapour in the feed mixtures, which implies that the measurements were performed at variable pressures of the fed vapour mixtures. To reflect this variability of feed pressure and to compare the state of the fed vapour with that of liquid, the ratio of such pressure of vapours to the dew point pressure [15] is shown in Table 3. Permeabilities increased with increasing activity of MeOH vapours as well as with increasing ratio of the pressure of the fed vapours and dew point pressure in most cases; decreasing permeabilities were observed for increasing methanol activity at 0.82 mol.% of MeOH for CTA. Consistent with that, the permeabilities measured by pervaporation of liquids were by ca. two orders of magnitude higher than those obtained for the vapour permeation while the separation factors were significantly smaller than those observed for vapours (Table 4). Hence, it follows that neither pervaporation nor vapour permeation was highly selective and highly intensive at the same time. Based on the preliminary tests, pervaporation did not show significant separation factors for the CTA membrane, which were also not enhanced upon blending CTA with PBS; only selected blends were thus characterized. In Fig. 11, McCabe-Thiele "y-x" diagrams are shown for vapour-liquid equilibrium, permeation of vapours and pervaporation. Clearly, the better separation of the azeotrope was achieved by permeation of diluted vapours (*i.e.* at small methanol vapour activity).

Table 4
Permeabilities (Eq. (2)) and separation factors (Eq. (6)) of CTA and PBS-CTA blends for liquid MeOH-DMC mixtures of given composition; all at 40 °C.

	x_{MeOH} [−]	P_{MeOH} [Barrer]	P_{DMC} [Barrer]	β_{MeOH} [−]
CTA	0.53	$2.1\ 10^5$	$6.5\ 10^5$	1.51
	0.66	$1.0\ 10^5$	$1.4\ 10^5$	1.32
	0.77	$8.8\ 10^4$	$9.9\ 10^4$	1.08
	0.83	$7.2\ 10^4$	$7.5\ 10^4$	1.02
CTA + 10 wt% PBS	0.68	$6.0\ 10^4$	$7.9\ 10^4$	0.76
	0.88	$3.7\ 10^4$	$3.4\ 10^4$	1.07
	0.87	$1.6\ 10^4$	$1.2\ 10^4$	1.38
	0.95	$1.1\ 10^4$	$4.9\ 10^3$	2.29
CTA + 30 wt% PBS	0.48	$5.7\ 10^4$	$1.0\ 10^5$	1.65
	0.63	$5.3\ 10^4$	$6.1\ 10^4$	1.58
	0.71	$4.4\ 10^4$	$5.3\ 10^4$	1.20
	0.83	$3.7\ 10^4$	$3.5\ 10^4$	1.01
	0.95	$2.9\ 10^4$	$1.8\ 10^4$	1.01

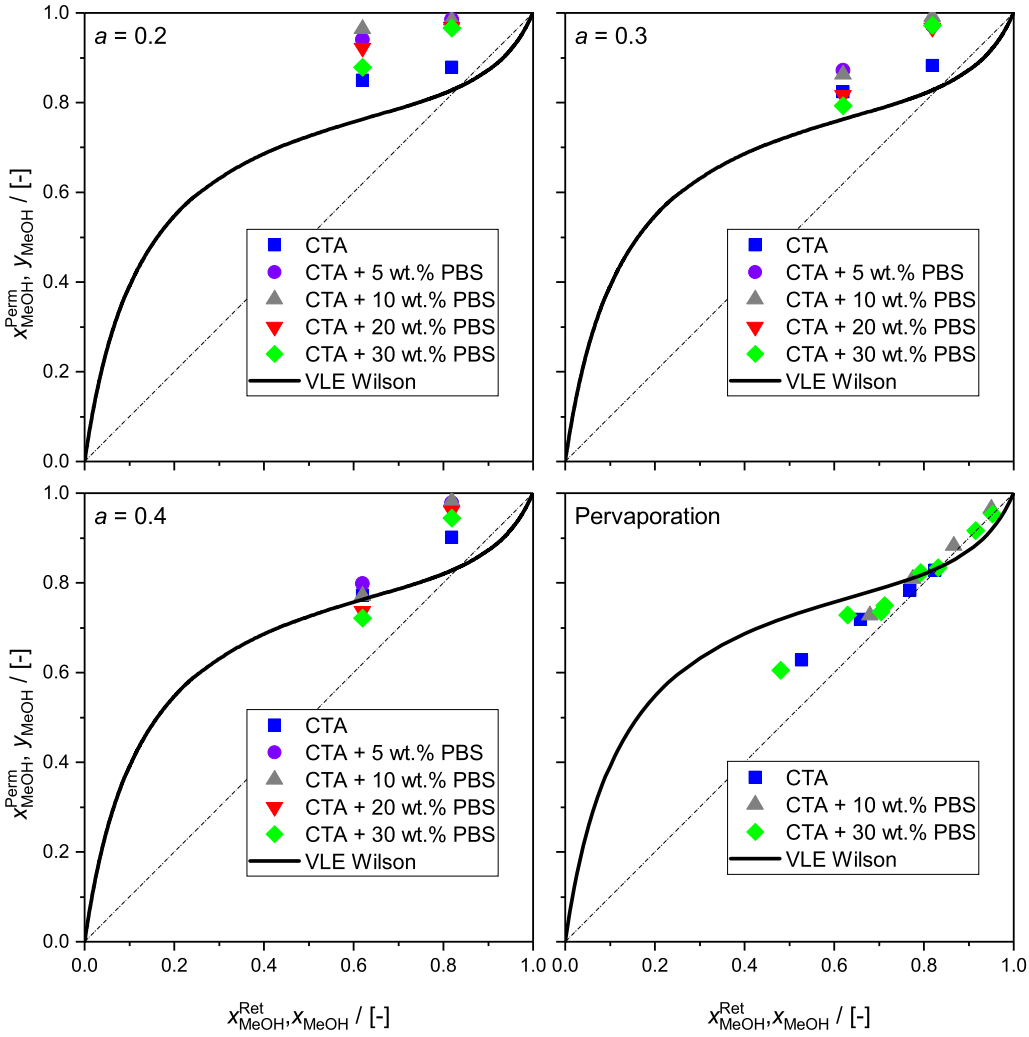

Fig. 11. The "*y-x*" diagram for the permeation of vapours (for three activities of methanol vapour in the feed) and for pervaporation through PBS-CTA blends and through CTA. Data for vapour-liquid equilibrium [15] are shown for comparison.

Similar behaviour was earlier observed for numerous dehydration membranes [4] and presumably originates from the more extensive plasticization of the membranes in the case of pervaporation. Overall, films from PBS-CTA blends are less permeable but more selective towards methanol than CTA films, particularly when used as vapour permeation membranes.

4.4. Sorption of vapours

To thoroughly survey their transport properties, sorption of vapours in flat films from the PBS-CTA blends was studied by means of sorption microgravimetry at 40 °C. Equilibrium sorption isotherms of MeOH, DMC and MeOAc in CTA, PBS and their blends are shown in Figs. 12–14, together with the respective diffusivities calculated from

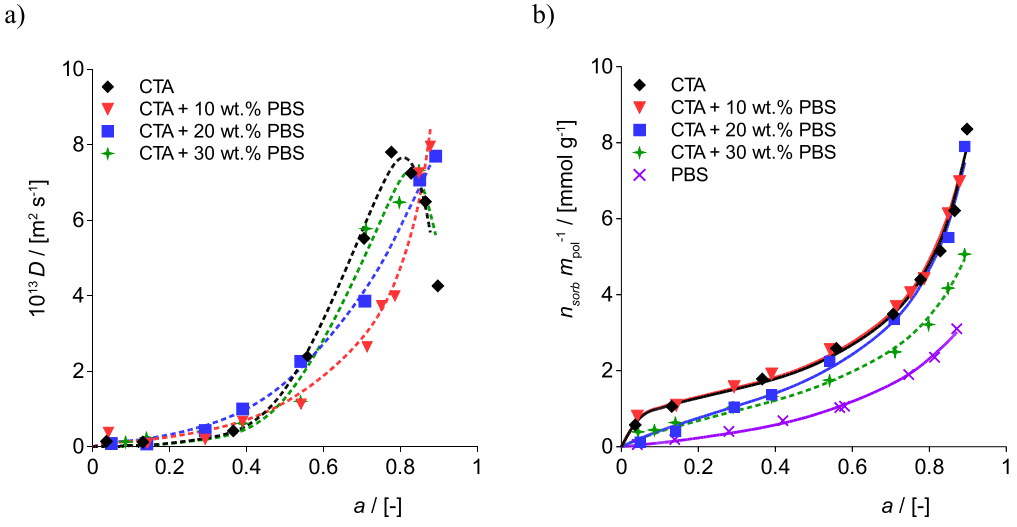

Fig. 12. Diffusivities (a) and sorption uptakes (b) of DMC as functions of vapour activity at 40 °C. Solid lines represents GAB model fit with PBS amount dependence (coefficients in Table 5) and dashed lines are trend lines. In the case of sorption in CTA with 30 wt% of PBS (b), GAB model with parameters with v_m = 1.06 mmol g^{-1}, h = 5.25 and f = 0.89 was used.

the transient sorption using Eq. (3), in which correction to real time dependence of sorbate pressure was used as described earlier in the literature [28]. Diffusivities of all studied compounds followed a similar upward-curved dependence on vapour activity, which was presumably so due to plasticization with the diffusing compounds. Diffusivities followed the expectable order MeOH > MeOAc > DMC, that is, lower diffusivities were observed for the bulkier compounds and higher for the less bulky ones. Consistent with that, diffusivities found at small vapour activities were of the order of $10^{-14}\,m^2\,s^{-1}$ for DMC and MeOAc, $10^{-13}\,m^2\,s^{-1}$ for MeOH. The drop of diffusivity, observed at high activities for some systems, was presumably a consequence of surface-mediated diffusion [39–41], which coheres with the applicability of GAB model of multilayer adsorption (see below), or of the formation of sorbate clusters [42,43]. Although diffusivities of the tested compounds in PBS were two orders of magnitude higher than those in CTA, diffusivities observed for the PBS-CTA blends practically equalled those for CTA. In contrast to that, the addition of PBS into CTA resulted to a clearly discernible drop of sorption uptakes of all tested compounds. Hence, the principal effect of PBS in its blends with CTA was the compound-specific reduction of sorption compared to that in pure CTA, while the diffusion path of the molecules within the matrix remained practically unchanged.

The dependences of the sorption uptakes in the blends on the vapour activities were well parameterized with GAB model of multilayer adsorption (4), the respective parameters are listed in Tables 5–7 together with the respective coefficients of determination and mean relative deviations (MRD) as defined in the literature [44]. Hence, sorption can be expected to have the nature of multilayer adsorption on the inner surfaces of the polymer matrix. Sorption isotherms of the two structural analogues, DMC and MeOAc, were of similar shape, while they differed from that of MeOH. In order to mimic the dependences of the parameters on the blend composition, empirical mixing rules have been proposed (Appendix I). Interestingly, sorption uptakes expressed in mole-based units were of comparable extent for all tested sorptives, which is in agreement with our earlier observations on sorption in pure CTA [29].

Besides the overall drop of sorption uptakes with the increasing amount of the PBS content, the principal change of the shape of the isotherms was identified. Indeed, sorption isotherms observed for pure CTA revealed a steep increase in the region of low vapour activities ([Figs. 12–14]) and thus were of type II according to IUPAC [45]. This steep increase was progressively reduced with the increasing PBS content, thus modifying the shape of the isotherms towards type III. This phenomenon resulted to the reduction of the binding strength parameter of GAB model (4), *i.e.* parameter *h*, which was higher for CTA and lower (close to unity) for PBS; see Tables 5–7. This was presumably a consequence of the filling or rearrangement of microstructures formed by CTA, which have the apparent spacing of 10.6 Å ($2\theta \approx 8°$); see Fig. 5. Interestingly, monolayer sorption capacity, v_m, was not significantly dependent either on the sorptive or on the PBS content in the blend, while rather moderate changes of the condensability parameter, *f*, were observed. Thus, the PBS chains weakened the strength of sorption of condensable molecules, thereby reducing the overall sorption uptakes, but did not extensively lower the monolayer sorption capacity. Seeing that together with the independences of the diffusion coefficient and glass transition temperature of the PBS content in the blend, it can be concluded that PBS chains act as a "molecular filler", while the principal properties of the blends remain most influenced by CTA. Generally, the reduction of sorption of condensable compounds might be valuable in applications, such as in the membrane sweetening of natural gas contaminated with glycols [9].

In order to disclose the influence of the intrinsic nanostructure of the blends on their properties, sorption uptakes of vapours were plotted against the area of the band peaking at $2\theta \approx 8°$ (apparent spacing 10.6 Å). Vapour sorption uptakes were clearly dependent on the integral of the XRD band and, to some extent, on the chemical structure of the testing compound. Besides that, the peak area clearly decreased with the PBS content (Fig. 15), thus implying that sorption of vapours as well as gas, vapour and liquid permeability can, in principle, be related either to the PBS content or to the area of the band. Hence, the main principle influencing sorption and mass transport in the blends is presumably the abundance of the inner structures, presumably voids, having of the apparent size of approx. 10.6 Å.

5. Conclusion

We report on the gas, vapour and liquid permeability of thin films prepared from blends of cellulose triacetate containing up to the 30 wt % of PBS, as well as on their thermal and mechanical properties and physical structure.

Physical structure and thermal and mechanical properties were studied using X-ray diffraction analysis, Scanning Electron Microscopy, Fourier transform infrared-attenuated total reflectance, Differential Scanning Calorimetry, Thermogravimetry and Dynamic Mechanical Analysis, conclusively showing that blends of PBS and CTA are homogenous, practically free from PBS crystallites and thermally soften at temperatures above ca. 125 °C when containing up to 30 wt% of PBS. Glass transition temperatures and elastic moduli of the blends similar to those of pure CTA, thus suggesting that the mechanical and thermal properties of the blends are most influenced by the CTA chains.

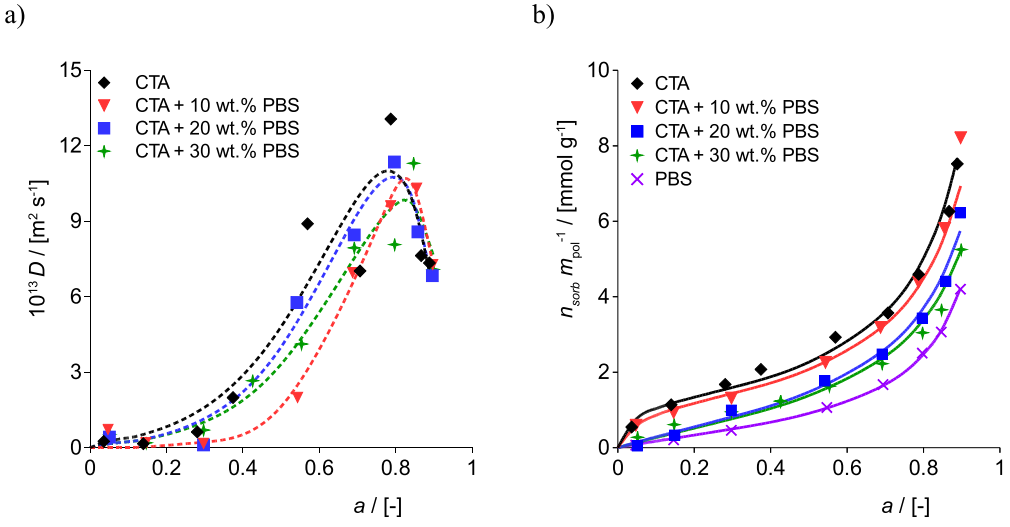

Fig. 13. Diffusivities (a) and sorption uptakes (b) of MeOAc as functions of vapour activity at 40 °C. Solid lines represents GAB model fit with PBS amount dependence (coefficients in Table 6) and dashed lines are trend lines.

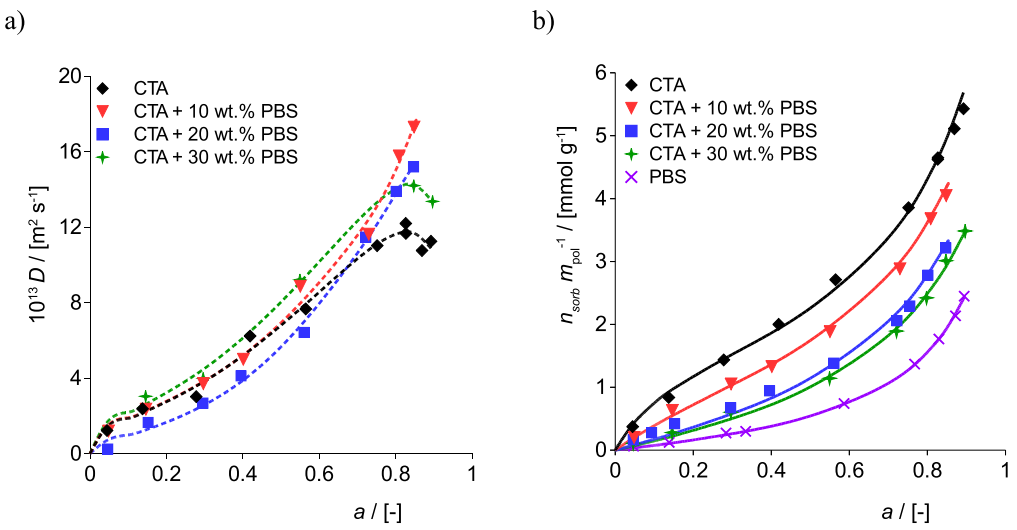

Fig. 14. Diffusivities (a) and sorption uptakes (b) of MeOH as functions of vapour activity at 40 °C. Solid lines represents GAB model fit with PBS amount dependence (coefficients in Table 7) and dashed lines are trend lines.

Table 5
Parameters of GAB model of DMC sorption in CTA, PBS and their blends together with the respective coefficients of determination and mean relative deviations (MRD) [44]. Correlation of parameters for blends containing up to 20 wt% of PBS (see Appendix I): A_h = 75.97, B_h = 0.186 and A_f = 1.91 (overall R^2 = 0.9982).

wt% of PBS	v_m/[mmol g^{-1}]	h/[−]	f/[−]	R^2	MRD
0 (pure CTA)	1.17	34.0	0.949	0.9915	0.053
10	1.20	34.0	0.949	0.9965	0.042
20	1.23	4.28	0.945	0.9920	0.184
30	1.06	5.25	0.891	0.9998	0.128
100 (pure PBS)	1.45	0.81	0.792	0.9972	0.097

Table 6
Parameters of GAB model of MeOAc sorption in CTA, PBS and their blends together with the respective coefficients of determination and mean relative deviations (MRD) [44]. Correlation of parameters for blends containing up to 30 wt% of PBS (see Appendix I): A_h = −99.4, B_h = 0.102 and A_f = 1.69 (overall R^2 = 0.9929).

wt% of PBS	v_m/[mmol g^{-1}]	h/[−]	f/[−]	R^2	MRD
0 (pure CTA)	1.24	29.7	0.945	0.9873	0.081
10	1.18	18.9	0.927	0.9657	0.055
20	1.12	3.00	0.913	0.9853	0.365
30	1.06	3.00	0.903	0.9790	0.154
100 (pure PBS)	0.652	3.00	0.952	0.9993	0.077

Table 7
Parameters of GAB model of MeOH sorption in CTA, PBS and their blends together with the respective coefficients of determination and mean relative deviations (MRD) [44]. Correlation of parameters for blends containing up to 30 wt% of PBS (see Appendix I): A_h = 15.65, B_h = 0.069 and A_f = 1.51 (overall R^2 = 0.9982).

wt% of PBS	v_m/[mmol g^{-1}]	h/[−]	f/[−]	R^2	MRD
0 (pure CTA)	1.53	8.96	0.831	0.9959	0.039
10	1.43	3.73	0.818	0.9738	0.052
20	1.33	1.54	0.809	0.9924	0.162
30	1.24	1.40	0.804	0.9973	0.111
100 (pure PBS)	0.562	1.40	0.898	0.9995	0.085

Depending on the probing compound, films prepared from the blends were up to two orders of magnitude less permeable than those prepared from pure CTA. Practically univocal drop of permeability was found for gases, thus leading to small changes of ideal selectivity occurring upon the addition of PBS. Conversely, the permeabilities of the films for methanol and dimethyl carbonate vapours changed compound-specifically, thus rendering the blends more selective towards methanol than pure CTA. In contrast to that, practically no

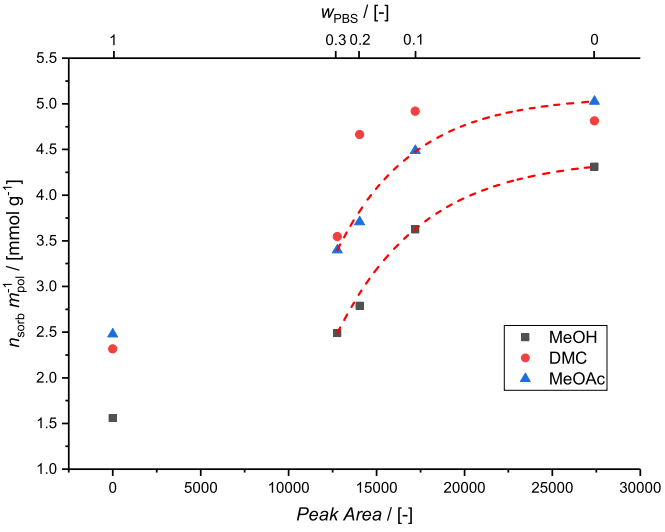

Fig. 15. Correlation of sorption uptakes of MeOH, MeOAc and DMC in CTA, PBS and their blends at the vapour activity a = 0.8 and at 40 °C. Peak area was calculated by integrating XRD signal from 5 to 11.5°; diffraction pattern of PBS was used as integration baseline. Dashed curves represent guides for the eye.

enhancement of separation was observed for the pervaporation of liquid mixtures of methanol and dimethyl carbonate upon the addition of PBS.

Sorption tests showed that the addition of PBS lowers the sorption uptakes of methanol, dimethyl carbonate and methyl acetate in the polymer phase, while it does not practically influence their diffusivities. Moreover, sorption isotherms showed non-trivial compound-specific dependences of the sorption uptakes on the PBS content. Sorption isotherms were thus analysed using GAB model of multilayer adsorption employing newly proposed empirical mixing rules. This analysis showed that blending of PBS into CTA primarily reduces sorption strength of condensable compounds, while it does not practically influence the monolayer sorption capacity. Overall, PBS chains presumably attach to the structures formed by CTA chains, thereby acting as a "molecular filler", while the principal properties of the blends remain most influenced by CTA.

Acknowledgment

Financial support obtained partly from the Czech Science Foundation under projects 13-32829P, 17-05421S, and from the Czech Ministry of Education, Youth and Sports (the specific university

research MSMT No 20/2016 and No 20/2017) are gratefully acknowledged. We also thank Martin Forejtová, Martina Kohoutková, Jakub Havlín and Monika Krejčí Slavíková for their help with the sorption, XRD and TGA measurements, and Kryštof Pilnáček for his help with the development of the gas permeation apparatus.

Nomenclature

a	Vapour activity
A	Membrane area
A_f, A_h, B_h, c_h, d_h	Empirical parameters and functions in mixing rules for GAB model, see Appendix I
β	Separation factor
γ	Activity coefficient
D	Diffusivity
E'	Elastic modulus
f	Condensability parameter
h	Sorption strength parameter
Δh	Specific enthalpy
J	Flux intensity
k	Empirical parameter, Eq. (7)
L	Thickness
m	Mass
p	Pressure or partial pressure
P	Permeability
R	Universal gas constant
t	Time
T	Temperature
$\tan\delta$	Damping
v	Sorption uptake
v_m	Monolayer sorption capacity
w	Mass fraction
x, y	Molar fractions
X_c	Crystallinity index
CTA	Cellulose triacetate
DMA	Dynamic mechanical analysis
DSC	Differential scanning calorimetry
FTIR-ATR	Fourier transform infrared-attenuated total reflectance
PBS	Poly(butylene succinate)
SEM	Scanning electron microscopy
TGA	Thermogravimetry
XRD	X-ray diffraction

Appendix I

Sorption of vapours in blends of PBS and CTA was well parameterized with Eq. (4), in which following empirical mixing rules were introduced:

$$v_m = v_m^{CTA}\,(1 - w_{PBS}) + v_m^{PBS}\,w_{PBS}, \tag{A1}$$

$$f = f^{CTA}\,(1 - w_{PBS})^2 + f^{PBS}\,w_{PBS}^2 - A_f\,w_{PBS}\,(1 - w_{PBS}), \tag{A2}$$

and

$$h = c_h\ \tanh[-A_h\ (w_{PBS} - B_h)] + d_h. \tag{A3}$$

A_h, A_f and B_h are empirical adjustable constants and c_h and d_h are constants which were introduced to comply with the following conditions: $h(w_{PBS} = 0) = h^{CTA}$ and $h(w_{PBS} = 1) = h^{PBS}$. These constants thus take the forms:

$$c_h = -\frac{1}{2}\frac{[(e^{A_h})^2(h^{PBS} - h^{CTA}) + (e^{A_hB_h})^2(h^{PBS} - h^{CTA})][(e^{A_hB_h})^2 + 1]}{(e^{A_hB_h})^2[(e^{A_h})^2 - 1]}, \tag{A4}$$

$$d_h = \frac{1}{2}\frac{(e^{A_h})^2(e^{A_hB_h})^2(h^{PBS} + h^{CTA}) + (e^{A_hB_h})^4(h^{PBS} - h^{CTA})}{(e^{A_hB_h})^2[(e^{A_h})^2 - 1]} - \frac{1}{2}\frac{(e^{A_h})^2(h^{PBS} - h^{CTA}) - (e^{A_hB_h})^2(h^{PBS} + h^{CTA})}{(e^{A_hB_h})^2[(e^{A_h})^2 - 1]}. \tag{A5}$$

References

[1] G. Wypych, 11.5 Cellulose acetate, Handbook of Plasticizers, third ed., ChemTec Publishing, 1995.
[2] J. Néel, Chapter 5 Pervaporation, in: R.D. Noble, S.A. Stern (Eds.), Membrane Science and Technology, vol. 2, Elsevier, 1995, pp. 143–211.
[3] K. Scott, Separation of liquid mixtures/pervaporation, Handbook of Industrial Membranes, Elsevier Science, Amsterdam, 1995, pp. 331–351.
[4] Y. Cen, R.N. Lichtenthaler, Chapter 3 Vapor permeation, in: R.D. Noble, S.A. Stern (Eds.), Membrane Science and Technology, vol. 2, Elsevier, 1995, pp. 85–112.
[5] K. Scott, Introduction to membrane separations, Handbook of Industrial

Membranes, Elsevier Science, Amsterdam, 1995, pp. 3–185.
[6] J. Li, K. Nagai, T. Nakagawa, S. Wang, Preparation of polyethyleneglycol (PEG) and cellulose acetate (CA) blend membranes and their gas permeabilities, J. Appl. Polym. Sci. 58 (9) (1995) 1455–1463.
[7] A.C. Puleo, D.R. Paul, S.S. Kelley, The effect of degree of acetylation on gas sorption and transport behavior in cellulose acetate, J. Membr. Sci. 47 (3) (1989) 301–332.
[8] F.Z. Khan, M. Shiotsuki, Y. Nishio, T. Masuda, Synthesis, characterization, and gas permeation properties of t-butylcarbamates of cellulose derivatives, J. Membr. Sci. 312 (1–2) (2008) 207–216.
[9] H.T. Lu, S. Kanehashi, C.A. Scholes, S.E. Kentish, The impact of ethylene glycol and hydrogen sulphide on the performance of cellulose triacetate membranes in natural gas sweetening, J. Membr. Sci. 539 (2017) 432–440.
[10] T. Uesaka, K. Nakane, S. Maeda, T. Ogihara, N. Ogata, Structure and physical properties of poly(butylene succinate)/cellulose acetate blends, Polymer 41 (23) (2000) 8449–8454.
[11] X. Wang, S. Huang, Y. Wang, P. Wei, Y. Chen, Y. Xia, Y. Wang, Eco-friendly cellulose acetate butyrate/poly(butylene succinate) blends: crystallization, miscibility, thermostability, rheological and mechanical properties, J. Polym. Res. 24 (2) (2017) 16.
[12] S.-H. Lee, S. Wang, Crystallization behaviour of cellulose acetate butylate/poly (butylene succinate)-co-(butylene carbonate) blends, Polym. Int. 55 (3) (2006) 292–298.
[13] R. Smith, Biodegradable Polymers for Industrial Applications, Taylor & Francis, 2005.
[14] D. Delledonne, F. Rivetti, U. Romano, Developments in the production and application of dimethylcarbonate, Appl. Catal. Gen. 221 (1–2) (2001) 241–251.
[15] F. Comelli, R. Francesconi, Isothermal vapor-liquid equilibria measurements, excess molar enthalpies, and excess molar volumes of dimethyl carbonate + methanol, + ethanol, and + propan-1-ol at 313.15 K, J. Chem. Eng. Data 42 (4) (1997) 705–709.
[16] R.W. Baker, B.T. Low, Gas separation membrane materials: a perspective, Macromolecules 47 (20) (2014) 6999–7013.
[17] J.G. Wijmans, R.W. Baker, The solution-diffusion model: a review, J. Membr. Sci. 107 (1) (1995) 1–21.
[18] J. Crank, The Mathematics of Diffusion, second ed., Clarendon Press, 1975.
[19] R.W. Baker, J.G. Wijmans, Y. Huang, Permeability, permeance and selectivity: a preferred way of reporting pervaporation performance data, J. Membr. Sci. 348 (1) (2010) 346–352.
[20] O. Vopička, A. Randová, K. Friess, Sorption of vapours and liquids in PDMS: novel data and analysis with the GAB model of multilayer adsorption, Eur. Polym. J. 60 (2014) 49–57.
[21] O. Vopička, K. Pilnáček, P. Číhal, K. Friess, Sorption of methanol, dimethyl carbonate, methyl acetate, and acetone vapors in CTA and PTMSP: general findings from the GAB Analysis, J. Polym. Sci. B Polym. Phys. 54 (5) (2016) 561–569.
[22] E.A. Guggenheim, Application of Statistical Mechanics, Clarendon Press, Oxford, 1966.
[23] J.L. Braun, J.F. Kadla, CTA III: a third polymorph of cellulose triacetate, J. Carbohydr. Chem. 32 (2) (2013) 120–138.
[24] Design Institute for Physical Properties, S. b. A., DIPPR Project 801-Full Version. Design Institute for Physical Property Research/AIChE.
[25] K. Friess, P. Sysel, E. Minko, M. Hauf, O. Vopička, V. Hynek, K. Pilnáček, M. Šípek, Comparison of transport properties of hyperbranched and linear polyimides, Desalination Water Treat. 14 (1–3) (2010) 165–169.
[26] O. Vopička, K. Pilnáček, K. Friess, Separation of methanol-dimethyl carbonate vapour mixtures with PDMS and PTMSP membranes, Separ. Purif. Technol. 174 (2017) 1–11.
[27] O. Vopička, D. Radotínský, K. Friess, Sorption of vapour mixtures of methanol and dimethyl carbonate in PDMS: experimental study, Eur. Polym. J. 73 (2015) 480–486.
[28] P. Číhal, O. Vopička, K. Pilnáček, J. Poustka, K. Friess, J. Hajšlová, J. Dobiáš, P. Dole, Aroma scalping characteristics of polybutylene succinate based films, Polym. Test. 46 (2015) 108–115.
[29] O. Vopička, K. Pilnáček, P. Číhal, K. Friess, Sorption of methanol, dimethyl carbonate, methyl acetate, and acetone vapors in CTA and PTMSP: general findings from the GAB Analysis, J. Polym. Sci. B Polym. Phys. 54 (5) (2016) 561–569.
[30] T. Dong, Y. He, K.M. Shin, Y. Inoue, Formation and characterization of inclusion complexes of poly(butylene succinate) with alpha- and gamma-cyclodextrins, Macromol. Biosci. 4 (12) (2004) 1084–1091.
[31] L. Li, G. Song, G. Tang, Novel biodegradable polylactide/poly(butylene succinate) composites via cross-linking with methylene diphenyl diisocyanate, Polym. Plast. Technol. Eng. 52 (12) (2013) 1183–1187.
[32] S.-F. Yao, X.-T. Chen, H.-M. Ye, Investigation of structure and crystallization behavior of poly(butylene succinate) by Fourier transform infrared spectroscopy, J. Phys. Chem. B 121 (40) (2017) 9476–9485.
[33] W.F. Yong, Z.K. Lee, T.-S. Chung, M. Weber, C. Staudt, C. Maletzko, Blends of a polymer of intrinsic microporosity and partially sulfonated polyphenylenesulfone for gas separation, ChemSusChem 9 (15) (2016) 1953–1962.
[34] G. Bengtson, S. Neumann, V. Filiz, Membranes of polymers of intrinsic microporosity (PIM-1) modified by poly(ethylene glycol), Membranes 7 (2) (2017) 28.
[35] P. Salehian, W.F. Yong, T.-S. Chung, Development of high performance carboxylated PIM-1/P84 blend membranes for pervaporation dehydration of isopropanol and CO2/CH4 separation, J. Membr. Sci. 518 (2016) 110–119.
[36] K. Halder, M.M. Khan, J. Grünauer, S. Shishatskiy, C. Abetz, V. Filiz, V. Abetz, Blend membranes of ionic liquid and polymers of intrinsic microporosity with improved gas separation characteristics, J. Membr. Sci. 539 (2017) 368–382.
[37] I. Pinnau, C.G. Casillas, A. Morisato, B.D. Freeman, Hydrocarbon/hydrogen mixed gas permeation in poly(1-trimethylsilyl-1-propyne) (PTMSP), poly(1-phenyl-1-propyne) (PPP), and PTMSP/PPP blends, J. Polym. Sci. B Polym. Phys. 34 (15) (1996) 2613–2621.
[38] L.M. Robeson, The upper bound revisited, J. Membr. Sci. 320 (1–2) (2008) 390–400.
[39] Y. Chen, R.T. Yang, Surface and mesoporous diffusion with multilayer adsorption, Carbon 36 (10) (1998) 1525–1537.
[40] S.W. Rutherford, Mechanism of sorption and diffusion in a high free-volume polymer, Ind. Eng. Chem. Res. 40 (5) (2001) 1370–1376.
[41] J.M. Watson, G.S. Zhang, P.A. Payne, The diffusion mechanism in silicone rubber, J. Membr. Sci. 73 (1) (1992) 55–71.
[42] E. Favre, P. Schaetzel, Q.T. Nguygen, R. Clément, J. Néel, Sorption, diffusion and vapor permeation of various penetrants through dense poly(dimethylsiloxane) membranes: a transport analysis, J. Membr. Sci. 92 (2) (1994) 169–184.
[43] Y. Sun, S.J. Harley, E.A. Glascoe, Modeling and uncertainty quantification of vapor sorption and diffusion in heterogeneous polymers, ChemPhysChem 16 (14) (2015) 3072–3083.
[44] S. Basu, U.S. Shivhare, A.S. Mujumdar, Models for sorption isotherms for foods: a review, Dry. Technol. 24 (8) (2006) 917–930.
[45] K.S.W. Sing, D.H. Everett, R.A.W. Haul, L. Moscou, R.A. Pierotti, J. Rouquerol, T. Siemieniewska, Reporting physisorption data for gas/solid systems with special reference to the determination of surface area and porosity, Pure Appl. Chem. 57 (4) (1985) 603–619.